Correlation-enhanced neural networks as interpretable variational quantum states

Valenti, Agnes; Greplova, Eliska; Lindner, Netanel H.; Huber, Sebastian D.

DOI
10.1103/PhysRevResearch.4.L012010

Publication date
2022

Document Version
Final published version

Published in
Physical Review Research

Letter

Correlation-enhanced neural networks as interpretable variational quantum states

Agnes Valenti,[1] Eliska Greplova,[1,2] Netanel H. Lindner,[3] and Sebastian D. Huber[1]
[1]*Institute for Theoretical Physics, ETH Zurich, CH-8093 Zurich, Switzerland*
[2]*Kavli Institute of Nanoscience, Delft University of Technology, NL-2600 GA Delft, The Netherlands*
[3]*Physics Department, Technion, Haifa 3200003, Israel*

(Received 10 March 2021; revised 13 January 2022; accepted 14 January 2022; published 31 January 2022)

Variational methods have proven to be excellent tools to approximate the ground states of complex many-body Hamiltonians. Generic tools such as neural networks are extremely powerful, but their parameters are not necessarily physically motivated. Thus, an efficient parametrization of the wave function can become challenging. In this Letter we introduce a neural-network-based variational ansatz that retains the flexibility of these generic methods while allowing for a tunability with respect to the relevant correlations governing the physics of the system. We illustrate the success of this approach on topological, long-range correlated, and frustrated models. Additionally, we introduce compatible variational optimization methods for the exploration of low-lying excited states without symmetries that preserve the interpretability of the ansatz.

DOI: 10.1103/PhysRevResearch.4.L012010

Studying many-body systems beyond analytically solvable Hamiltonians is a formidable challenge due to the exponential growth of the Hilbert space size with the number of particles. While quantum Monte Carlo methods offer an unbiased solution to that challenge, they are not applicable to systems exhibiting the notorious sign problem [1–3]. For models where numerically exact methods are not available, we can resort to variational methods: A clever parametrization of trial wave functions allows us to capitalize on physical intuition. This approach has led to scientific breakthroughs such as the Bardeen-Cooper-Schrieffer theory of superconductivity [4]. More sophisticated approaches were developed based on the same principle of using knowledge about the system's physics to obtain an accurate parametrization. Examples include Slater-Jastrow [5,6] or Gutzwiller-projected wave functions [2,7–12]. While these ansätze are able to represent also highly correlated states parametrized in an interpretable way, their simplicity comes with limited variational freedom.

Instead of starting from a system-specific wave function, other more universal approaches have been developed that rely on a generic parametrization of a submanifold of the Hilbert space. Typically, the size of the spanned subspace is controlled via a tuning parameter determining the number of optimizable variables and thereby the wave-function accuracy. An example of this class are tensor-network states (TNS), which span a submanifold of the Hilbert space determined by specific entanglement properties [13–25]. More recently, neural-network-based variational ansätze have been brought forward, providing a flexible wave-function ansatz not limited by entanglement or dimensionality [26]. Proposed architectures include restricted Boltzmann machines (RBMs) [26] or feed-forward (convolutional) neural networks [27–30]. Neural-network ansätze have been successfully applied to a range of different bosonic as well as fermionic systems [29,31–47]. While in principle highly expressive and efficiently trainable, previously proposed neural-network architectures suffer from the fact that their parameters are often not physically motivated or interpretable, such that an efficient representation of the sought-after wave function is not ensured. As a consequence, an exponential number of parameters might be required to obtain high-accuracy wave functions [48]. Especially for applications such as the study of (topological) quantum phase transitions or identification of excited states, this exponential scaling represents a significant challenge.

Here, we propose a variational ansatz that combines the advantages of both physically motivated and generic variational methods while at the same time combating their respective limitations. In particular, we design a neural-network variational ansatz that is explicitly customizable to the form of the expected dominant correlations of the system under consideration. To this end, we extend the energy functional describing an RBM by introducing coupling terms reflecting physical intuition. The inclusion of such correlators leads to a significant increase in the precision and flexibility of neural nets, while keeping the number of optimizable parameters minimal. Moreover, we show that these correlated RBMs (cRBMs) can capture ground and low-energy excited states equally well: We formulate a variational approach to obtain excited states without symmetries that does not modify the structure of the ansatz and thus preserves the interpretability of the variational wave function.

Before we discuss the performance of the cRBM variational ansätze on concrete examples, we note that by generalizing the class of RBM wave functions, we can in

principle describe systems outside the reach of quantum Monte Carlo techniques (e.g., systems suffering from a sign problem [3,49–52]) or tensor-network approaches (e.g., chiral topological phases, or systems in three and higher dimensions [34,53,54]).

We demonstrate the power of the cRBM variational ansatz by providing a complete description of the phase diagram of a model showcasing topological transitions: Kitaev's toric model in the presence of magnetic fields [55–59]. We further demonstrate the interpretability of our ansatz by linking the improved accuracy of the correlation functions to the customized physical extension of the energy functional on a long-range correlated model, the transverse field Ising model at criticality. Finally, we evaluate the performance of the ansatz on the antiferromagnetic Heisenberg model on a triangular lattice. In particular, we show that introducing coupling terms in the RBM ansatz can be used as a generic extension alternatively to increasing the hidden neuron density.

Toric code model. We explain the main properties of the cRBM ansatz on the perturbed toric code model with periodic boundary conditions [55] described by the Hamiltonian

$$H = -\sum_s A_s - \sum_p B_p + \vec{h} \cdot \sum_i \vec{\sigma}_i, \tag{1}$$

where $\vec{\sigma}_i$ denotes the Pauli matrices $\vec{\sigma}_i = (\sigma_i^x, \sigma_i^y, \sigma_i^z)$. The stabilizer operators $A_s = \prod_{i \in s} \sigma_i^x$ and $B_p = \prod_{i \in p} \sigma_i^z$ mutually commute. Vertices (plaquettes) of a square lattice are denoted by the subscripts s (p) and i runs over the edges, where spin-1/2 degrees of freedom are located. We apply a magnetic field $\vec{h} = (h_x, h_y, h_z)$ uniformly on each spin.

For $\vec{h} = 0$, Hamiltonian (1) corresponds to the well-understood toric code, where in the ground state all operators A_s and B_p yield an eigenvalue $+1$ [55]. This phase possesses topological order characterized by a fourfold degenerate ground state on a torus.

The applied magnetic fields induce a phase transition out of the topologically protected phase. The nature and position of this transition depend on the direction of the applied field. While the magnetic fields h_x and h_z are responsible for a second-order topological phase transition, a first-order phase transition occurs when the transverse field h_y dominates [52,60].

The phase diagram (see Fig. 1) has been previously explored by a variety of methods, but providing a unified approach capturing all features of this phase diagram has proven to represent a particular challenge. Numerically exact quantum Monte Carlo methods are only applicable to fields $\vec{h} \propto (h_x, 0, h_z)$, i.e., parallel to the operators A_s, B_p in (1) [61,62]. One can circumvent this restriction by using either approximate methods such as advanced perturbation theory or by resorting to a specific class of variational wave functions in the form of infinite projected entangled pair states [52,60,63]. In what follows, we show that the cRBM ansatz is able to capture the complete phase diagram.

cRBM structure. We introduce our proposed family of variational wave functions and highlight the differences to existing approaches. After exposing how to tailor the ansatz to a specific problem at hand we elaborate on how to determine the variational parameters.

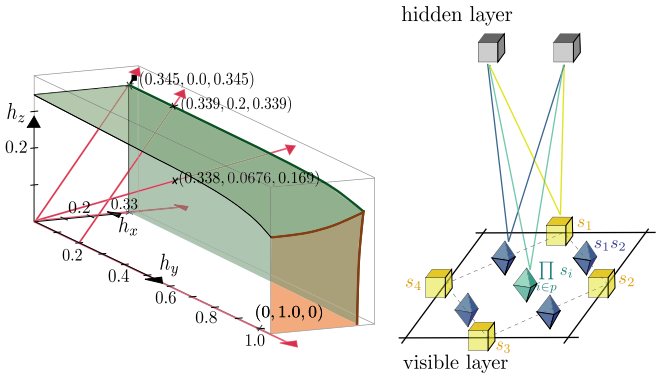

FIG. 1. Left: Conceptual phase diagram of the toric code. The red arrows show field directions in which we probed the diagram and the coordinates denote the obtained positions of the phase transition. The right panel shows the conceptual cRBM structure for a plaquette of the toric code model. Blue and green neurons and their connections to the hidden layer represent the added correlation terms.

We consider a system of N spin-1/2 degrees of freedom. In Ref. [26], Carleo and collaborators introduced RBMs as a variational ansatz for such a system,

$$\Psi(s_1, \ldots, s_N) = \sum_{\vec{\rho}} \exp[E_{\mathrm{RBM}}(\Lambda)],$$
$$E_{\mathrm{RBM}}(\Lambda) = \sum_k a_k s_k + \sum_j b_j \rho_j + \sum_{k,j} W_{k,j} s_k \rho_j, \tag{2}$$

where the $s_k \in \{-1, 1\}$ represent the physical spins in a given basis and, in the language of RBMs, are termed the *visible layer*. The wave-function ansatz $\Psi(s_1, \ldots, s_N)$ includes a sum over all possible values of the M auxiliary spins $\vec{\rho} = (\rho_1, \ldots, \rho_M)$, $\rho_i \in \{-1, 1\}$, denoted as the *hidden layer*. The energy functional $E_{\mathrm{RBM}}(\Lambda)$ can be understood as an interaction energy between classical spins. The parametrization $\Lambda = (\mathbf{a}, \mathbf{b}, W)$ includes visible and hidden biases a_k and b_j as well as weights $W_{k,j}$ connecting the visible and hidden layer.

RBMs have been shown to represent exactly a wide class of topological states, including the unperturbed toric code ground state [64]. Here, we investigate to which extent modifications of RBMs are able to capture both extensions of the toric code as in (1) as well as systems where no exact RBM representation exists for any point of the phase diagram.

We modify the RBM ansatz by introducing *correlators to the energy functional* (2). We achieve this by adding visible neurons to the ansatz representing correlations between different spins. Concretely, the modification yields the energy functional

$$E(\Lambda) = E_{\mathrm{RBM}}(\Lambda) + \sum_i a_i^{\mathrm{corr}} C_i + \sum_{i,j} W_{i,j}^{\mathrm{corr}} C_i \rho_j, \tag{3}$$

where $C_i = s_l \cdots s_k$ are products between spins chosen to reflect dominant terms influencing the system's behavior. The sum i runs over possible sets of spins entering the correlator C_i. These additional visible neurons are accompanied by their own biases and weights representing the interactions with the auxiliary spins of the hidden layer as shown in Fig. 1. Equation (3) represents the key idea of this Letter.

The types of correlators $C_i = s_l \cdots s_k$ that are added to the visible layer determine the efficiency of the use of the parameters in Λ. Moreover, it is in the design of these correlators, where the power of the cRBMs in allowing for the use of prior knowledge about the structure of the wave function can be capitalized on. In the spirit of conventional Jastrow-factor wave functions, the choice $C_i = s_l s_k$ representing two spin correlators can improve the wave-function accuracy without an exponential growth in the number of hidden neuron densities. Moreover, for specific problems we can include more complex terms. For example, in the case of the Hamiltonian (1) the relevance of plaquette operators can be mirrored on the level of the wave function by including toric code stabilizer operators $C_p = B_p = \prod_{i\in p} s_i$ in the energy functional. These extensions are depicted in Fig. 1. In order to further reduce the number of parameters and achieve higher precision, we symmetrize the ansatz (3) using translational symmetries as is usually done [26]. The details of the ansatz and imposed symmetries are further specified in the Supplemental Material (SM) [65].

We fix the weights in Λ by minimizing the cost function $\mathcal{C}$ corresponding to the variational energy

$$\mathcal{C} := \langle E \rangle = \frac{\langle \Psi | H | \Psi \rangle}{\langle \Psi | \Psi \rangle} \tag{4}$$

using a stochastic reconfiguration, introduced by Sorella *et al.* [66]. Expectation values are then calculated using variational Monte Carlo sampling [65–68]. Computations using the standard RBM as comparison have been partly done with the help of the library NETKET [69].

Results. We now turn to the application of cRBMs to the investigation of the Hamiltonian (1). First, we assess the accuracy of our wave function by benchmarking it against exact results for small system sizes. In particular, we emphasize the scaling of the accuracy with the number of variational parameters. To explore larger system sizes we compare our wave function with state-of-the art perturbation theory.

One can quantify the precision of the variational energy E_{var} by comparing it with the exact value E_{ED} obtained by exact diagonalization (ED) of Hamiltonian (1) on small lattices. We choose a lattice with $N = 18$ spins, and compare the relative error $\nu = (E_{\text{var}} - E_{\text{ED}})/E_{\text{ED}}$ using a standard RBM ansatz with $\alpha = 7$, where α corresponds to the number of hidden neurons. We compare it to a cRBM ansatz with the same amount of parameters (corresponding to $\alpha = 2$). As shown in Fig. 2, ν of the cRBM ansatz is several orders of magnitude lower than the relative error obtained using the standard RBM ansatz. As demonstrated in the SM [65], here the variational energy of the standard RBM ansatz cannot be significantly improved by increasing the hidden neuron density. Hence, the addition of the correlator terms in (3) allows us to explore the relevant section of the Hilbert space more efficiently.

We examine the performance of our ansatz for larger system sizes by comparing to state-of-the-art perturbation theory results using perturbative continuous unitary transformations (PCUTs) [52,63]. For a lattice with $N = 128$ spins the variational and perturbative energies for the magnetic field $(h, 0, 0)$ are compared in Fig. 2. The second-order phase transition for the chosen field direction is known to occur at $h_c = 0.3284$ and the perturbation theory we compare to in Fig. 2 is know

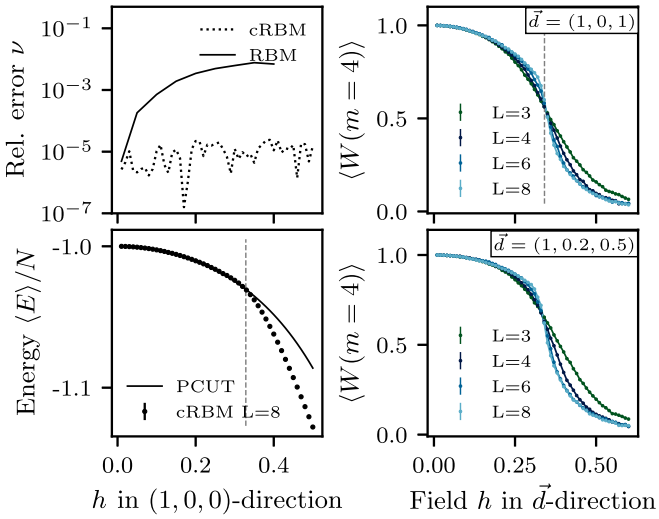

FIG. 2. Upper left: Relative error of the variational energy ν vs the field h for 18 spins. Lower left: The energy per spin for the cRBM ansatz for 128 spins is shown together with the energy per spin obtained via PCUTs. Upper right: Wilson loop expectation values $\langle W(m=4)\rangle$ on the self-dual line for different lattice sizes cross at the position of the phase transition. The literature value obtained via continuous-time Monte Carlo [62] is marked with a gray dashed line. Lower right: $\langle W(m=4)\rangle$ for fields in the (1,0.2,0.5) direction.

to be reliable for $h < h_c$. Figure 2 confirms that the variational energies match the perturbative energies well up to the second-order phase transition, while yielding more accurate results outside of the topological phase.

We can now use the cRBM ansatz to detect topological phase transitions. In particular, we probe the toric code in arbitrary field directions in order to recover the phase diagram, as depicted in Fig. 1. We are not limited to specific field directions as neither a sign problem occurs compared to quantum Monte Carlo methods [62], nor is the method restricted to a specific type of phase transition [52,63,70]. We demonstrate our results on the self-dual line $(h, 0, h)$ and a ray including a generic field direction $h(1, 0.2, 0.5)$. Recovering the characteristics of the self-dual line represents a particular challenge due to an occurring multicritical point and a first-order transition line outside of the topological phase [61,62]. We detect the position of the topological phase transition in both cases using a finite-size scaling analysis of the Wilson loop

$$\langle W(m) \rangle = \left\langle \prod_s^m A_s \prod_p^m B_p \right\rangle, \tag{5}$$

where m determines the size of the loop.

Figure 2 shows the expectation value $\langle W(m=4)\rangle$ versus the magnitude of the applied field for system sizes up to $N = 128$ spins. The curves for different system sizes cross approximately at the position of the phase transition which can be determined via a standard finite-size scaling analysis. We estimate the phase transition on the self-dual line $(h, 0, h)$ to occur at $h \sim 0.345$, which is in accordance to literature values [62,63] (see SM [65]). For the field direction $h(1, 0.2, 0.5)$, we obtain a transition at $h \sim 0.338$. We confirm in the SM

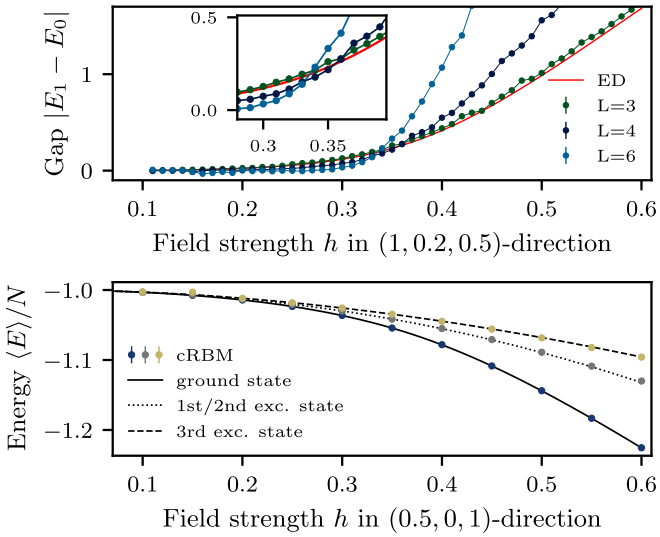

FIG. 3. Upper panel: The gap $|E_1 - E_0|$ to the first excited state is shown for the lattice sizes $L = 3, 4, 6$. For $L = 3$, the gap obtained via ED is plotted as a red line. The phase transition occurs at the crossing of the gaps for different lattice sizes (inset), since topological ground-state degeneracy in the thermodynamic limit only holds in the topological phase. Lower panel: The four lowest-lying ground states obtained via ED (lines) and with constrained cRBM (dots) for $L = 3$. The three colors correspond to the different topological sectors.

[65] the found phase transitions by computing the *fidelity*, the overlap between two ground states with a small difference in field strength that has been shown to scale to zero at the position of a second-order quantum phase transition [71–74]. Long-range entanglement in the topological phase is found by probing the Renyi entanglement entropy [75] (see SM [65]).

Excited states. We have shown that our ansatz can represent the ground state of the studied topological model to high precision. However, relevant physics such as the splitting of topological degeneracies and excitations are encoded in the low-energy spectrum. Obtaining excited states with an unknown quantum number poses a general challenge for variational wave functions [30]. We propose here a generic solution to this challenge that preserves the cRBM structure and flexibility of our ansatz. In particular, we add the required orthogonality to the ground state we have previously found as a constraint to the cost function for the optimization of the wave function

$$\mathcal{C} = \frac{\langle \Psi | H | \Psi \rangle}{\langle \Psi | \Psi \rangle} + \kappa \frac{|\langle \Psi_0 | \Psi \rangle|^2}{\langle \Psi_0 | \Psi_0 \rangle \langle \Psi | \Psi \rangle}, \tag{6}$$

where $|\Psi\rangle$ corresponds to the excited state to be optimized and $|\Psi_0\rangle$ is the ground-state approximation determined in a previous step. The parameter κ tunes the strength of the added constraint. The excited state is then obtained by minimizing the cost function using again stochastic reconfiguration. Extending the cost function while keeping the wave-function ansatz intact allows us to fully capitalize on the physically motivated ansatz as it preserves the wave-function structure.

We compute the gap between the ground state and the first excited state for the field $h(1, 0.2, 0.5)$, as depicted in Fig. 3. The energy gap quantitatively matches the exact diagonalization result for small system sizes. Scaling of the energy gap unravels the topological degeneracy: The gap scales with system size as e^{-L} (see SM [65]).

We introduce a further generalization of the cost function that allows for targeting specific states and does not rely on ground-state orthogonalization. In particular, when considering a generic operator M, it is straightforward to obtain the state with the lowest variational energy fulfilling the constraint $\langle M \rangle = A$ by minimizing the cost function

$$\mathcal{C} = \frac{\langle \Psi | H | \Psi \rangle}{\langle \Psi | \Psi \rangle} + \kappa \left| \frac{\langle \Psi | M | \Psi \rangle}{\langle \Psi | \Psi \rangle} - A \right|^2 \tag{7}$$

for sufficiently large weight κ and arbitrary constant A. This constrained minimization allows us to "cherry-pick" for an eigenstate with certain physical quantities. We can, e.g., consider the four lowest-lying eigenstates of the perturbed toric model. Operators yielding different expectation values for the four states can straightforwardly identified as loops Γ winding around the torus, as explained in the SM [65]. Minimizing (7) with $M = \Gamma$ for a sufficiently wide range of A and identifying eigenstates as the states with vanishing local energy variance or norm of variational energy derivatives [2] allows us to find all lowest-lying states of different topological sectors without the need to iteratively orthogonalize. Figure 3 depicts excited states found using this method and the cRBM ansatz for the field direction (0.5,0,1). Higher excited states such as anyonic excitations [55] can in principle be obtained by a suitable choice of operator M, e.g. stabilizers.

Transverse-field Ising model. We have shown on the example of the toric code, that introducing correlators tailored to the considered model to the energy functional increases the precision of the neural-network ansatz by several orders of magnitude. Additionally, let us demonstrate that the cRBM ansatz is also beneficial in a more general sense: We show that adding neurons representing generic correlations into the visible layer [as in Eq. (3)] rather than the hidden layer leads to a more efficient approximation of the sought-after wave function. In particular, we compare the effect of adding simple correlators $C_{i,j} = s_i s_j$ (with nearest-neighbor spins s_i and s_j) to the effect of increasing the hidden neuron density using the example of the transverse-field Ising model at the critical point [76,77].

The transverse-field Ising (TFI) model in one dimension (1D) is described by the Hamiltonian

$$H = -\sum_{\langle i,j \rangle} \sigma_i^z \sigma_j^z - h \sum_i \sigma_i^x, \tag{8}$$

where the sum runs over all nearest neighbors in the chain. The parameter h tunes the strength of the transverse field. At the critical point $h = 1$, the model exhibits long-range (algebraically decaying) spin-spin correlations [76,77].

In the standard RBM the spin-spin correlations are encoded in the sum over hidden neurons that forces the correlations to take a specific form (for details, see SM [65]). Using the cRBM extension, we are able to encode the spin-spin correlations in the visible layer allowing for increased flexibility of their representation. We show that this flexible encoding captures long-range correlations arising in the TFI model.

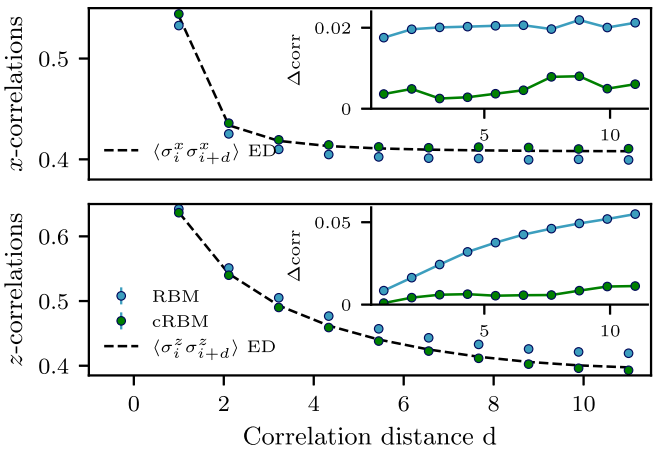

FIG. 4. 1D TFI correlations: z correlations and x correlations obtained with an RBM (blue) and cRBM (green) ansatz are plotted as a function of the correlation distance for $N = 22$ spins.

To make a simple comparison, we consider ansätze with a small hidden neuron density. In particular, we choose a standard symmetrized RBM ansatz [26] with $\alpha = 3$ hidden neurons and a cRBM with the same amount of parameters. Figure 4 shows the spin-spin correlation obtained for both variational wave functions. For both x and z correlations, the cRBM ansatz provides more accurate results. The most striking improvement appears for long-range z correlations, where z also corresponds to the choice of basis for the RBM (cRBM) ansatz. In the SM [65] we illustrate the above-mentioned improvement for the antiferromagnetic Heisenberg model on a triangular lattice [9–12,78–84] and we show that the improved accuracy of the cRBM ansatz can be further extended to frustrated systems.

Perspectives. We showed that a combination of generic neural-network-based ansätze and available knowledge about the system can lead to significant improvements in the precision of variational methods. We introduced a cRBM ansatz with a physically tunable flexibility and demonstrated its power on topological, long-range correlated, and frustrated models. In addition to formulating the cRBM ansatz we introduced compatible variational optimization techniques that allow for the study of the low-energy spectrum.

Neural-network-based ansätze have been shown to be applicable for systems outside the reach of TNS, such as chiral topological phases or systems in higher dimensions [34,53,54]. Mapping neural-network architectures to TNS explicitly demonstrates their ability to efficiently capture volume-law entanglement [33,34,85,86]. We generalize this mapping to the case of cRBMs in the SM [65]. We note, however, that while our cRBM approach can in principle be used for systems not accessible to TNS, the example of the generalized toric code studied here has an efficient tensor-network representation [52]. We leave studies of systems outside the realm of tensor networks to future studies.

In Ref. [87], we provide the code needed to calculate the energies and topological quantities from a pretrained cRBM wave function.

We are thankful for enlightening discussions with Eyal Bairey and Giacomo Torlai. We are grateful for financial support from the Swiss National Science Foundation, the NCCR QSIT. This work has received funding from the European Research Council under Grant Agreement No. 771503. N.L. acknowledges support from the Israel Science Foundation within the ISF-Quantum program (Grant No. 2074/19).

[1] D. Ceperley and B. Alder, Quantum Monte Carlo, Science **231**, 555 (1986).
[2] F. Becca and S. Sorella, *Quantum Monte Carlo Approaches for Correlated Systems* (Cambridge University Press, Cambridge, UK, 2017).
[3] M. Troyer and U.-J. Wiese, Computational Complexity and Fundamental Limitations to Fermionic Quantum Monte Carlo Simulations, Phys. Rev. Lett. **94**, 170201 (2005).
[4] J. Bardeen, L. N. Cooper, and J. R. Schrieffer, Theory of superconductivity, Phys. Rev. **108**, 1175 (1957).
[5] R. Jastrow, Many-body problem with strong forces, Phys. Rev. **98**, 1479 (1955).
[6] L. Mitáš and R. M. Martin, Quantum Monte Carlo of Nitrogen: Atom, Dimer, Atomic, and Molecular Solids, Phys. Rev. Lett. **72**, 2438 (1994).
[7] M. C. Gutzwiller, Effect of Correlation on the Ferromagnetism of Transition Metals, Phys. Rev. Lett. **10**, 159 (1963).
[8] C. Gros, Physics of projected wavefunctions, Ann. Phys. **189**, 53 (1989).
[9] D. Sheng, O. I. Motrunich, and M. P. A. Fisher, Spin Bose-metal phase in a spin-$\frac{1}{2}$ model with ring exchange on a two-leg triangular strip, Phys. Rev. B **79**, 205112 (2009).
[10] Y. Iqbal, F. Becca, and D. Poilblanc, Projected wave function study of $\mathbb{Z}_2$ spin liquids on the kagome lattice for the spin-$\frac{1}{2}$ quantum Heisenberg antiferromagnet, Phys. Rev. B **84**, 020407(R) (2011).
[11] S.-S. Gong, D. N. Sheng, O. I. Motrunich, and M. P. A. Fisher, Phase diagram of the spin-$\frac{1}{2}$ J_1-J_2 Heisenberg model on a honeycomb lattice, Phys. Rev. B **88**, 165138 (2013).
[12] W.-J. Hu, S.-S. Gong, W. Zhu, and D. N. Sheng, Competing spin-liquid states in the spin-$\frac{1}{2}$ Heisenberg model on the triangular lattice, Phys. Rev. B **92**, 140403(R) (2015).
[13] S. R. White, Density Matrix Formulation for Quantum Renormalization Groups, Phys. Rev. Lett. **69**, 2863 (1992).
[14] G. Vidal, Efficient Classical Simulation of Slightly Entangled Quantum Computations, Phys. Rev. Lett. **91**, 147902 (2003).
[15] G. Vidal, Entanglement Renormalization, Phys. Rev. Lett. **99**, 220405 (2007).
[16] F. Verstraete, M. M. Wolf, D. Perez-Garcia, and J. I. Cirac, Criticality, the Area Law, and the Computational Power of Projected Entangled Pair States, Phys. Rev. Lett. **96**, 220601 (2006).
[17] L. Vanderstraeten, M. Mariën, J. Haegeman, N. Schuch, J. Vidal, and F. Verstraete, Bridging Perturbative Expansions with Tensor Networks, Phys. Rev. Lett. **119**, 070401 (2017).

[18] R. Orús, A practical introduction to tensor networks: Matrix product states and projected entangled pair states, Ann. Phys. **349**, 117 (2014).
[19] D. Perez-Garcia, F. Verstraete, M. M. Wolf, and J. I. Cirac, Matrix product state representations, Quantum Inf. Comput. **7**, 401 (2007).
[20] F. Verstraete and J. I. Cirac, Valence-bond states for quantum computation, Phys. Rev. A **70**, 060302(R) (2004).
[21] Y.-Y. Shi, L.-M. Duan, and G. Vidal, Classical simulation of quantum many-body systems with a tree tensor network, Phys. Rev. A **74**, 022320 (2006).
[22] P. Silvi, V. Giovannetti, S. Montangero, M. Rizzi, J. I. Cirac, and R. Fazio, Homogeneous binary trees as ground states of quantum critical Hamiltonians, Phys. Rev. A **81**, 062335 (2010).
[23] G. Evenbly and G. Vidal, Entanglement Renormalization in Two Spatial Dimensions, Phys. Rev. Lett. **102**, 180406 (2009).
[24] A. J. Ferris, Area law and real-space renormalization, Phys. Rev. B **87**, 125139 (2013).
[25] T. Felser, S. Notarnicola, and S. Montangero, Efficient Tensor Network Ansatz for High-Dimensional Quantum Many-Body Problems, Phys. Rev. Lett. **126**, 170603 (2021).
[26] G. Carleo and M. Troyer, Solving the quantum many-body problem with artificial neural networks, Science **355**, 602 (2017).
[27] H. Saito, Solving the Bose–Hubbard model with machine learning, J. Phys. Soc. Jpn. **86**, 093001 (2017).
[28] H. Saito and M. Kato, Machine learning technique to find quantum many-body ground states of bosons on a lattice, J. Phys. Soc. Jpn. **87**, 014001 (2018).
[29] X. Liang, W.-Y. Liu, P.-Z. Lin, G.-C. Guo, Y.-S. Zhang, and L. He, Solving frustrated quantum many-particle models with convolutional neural networks, Phys. Rev. B **98**, 104426 (2018).
[30] K. Choo, G. Carleo, N. Regnault, and T. Neupert, Symmetries and Many-Body Excitations with Neural-Network Quantum States, Phys. Rev. Lett. **121**, 167204 (2018).
[31] X. Gao and L.-M. Duan, Efficient representation of quantum many-body states with deep neural networks, Nat. Commun. **8**, 1 (2017).
[32] Y. Nomura, A. S. Darmawan, Y. Yamaji, and M. Imada, Restricted Boltzmann machine learning for solving strongly correlated quantum systems, Phys. Rev. B **96**, 205152 (2017).
[33] J. Chen, S. Cheng, H. Xie, L. Wang, and T. Xiang, Equivalence of restricted Boltzmann machines and tensor network states, Phys. Rev. B **97**, 085104 (2018).
[34] I. Glasser, N. Pancotti, M. August, I. D. Rodriguez, and J. I. Cirac, Neural-Network Quantum States, String-Bond States, and Chiral Topological States, Phys. Rev. X **8**, 011006 (2018).
[35] G. Carleo, Y. Nomura, and M. Imada, Constructing exact representations of quantum many-body systems with deep neural networks, Nat. Commun. **9**, 5322 (2018).
[36] L. Pastori, R. Kaubruegger, and J. C. Budich, Generalized transfer matrix states from artificial neural networks, Phys. Rev. B **99**, 165123 (2019).
[37] D. Luo and B. K. Clark, Backflow Transformations Via Neural Networks for Quantum Many-Body Wave Functions, Phys. Rev. Lett. **122**, 226401 (2019).
[38] D. Kochkov and B. K. Clark, Variational optimization in the AI era: Computational graph states and supervised wave-function optimization, arXiv:1811.12423.
[39] F. Ferrari, F. Becca, and J. Carrasquilla, Neural Gutzwiller-projected variational wave functions, Phys. Rev. B **100**, 125131 (2019).
[40] D.-L. Deng, X. Li, and S. D. Sarma, Quantum Entanglement in Neural Network States, Phys. Rev. X **7**, 021021 (2017).
[41] N. Freitas, G. Morigi, and V. Dunjko, Neural network operations and Susuki–Trotter evolution of neural network states, Int. J. Quantum Inf. **16**, 1840008 (2018).
[42] Z. Cai and J. Liu, Approximating quantum many-body wave functions using artificial neural networks, Phys. Rev. B **97**, 035116 (2018).
[43] J. Han, L. Zhang, and E. Weinan, Solving many-electron Schrödinger equation using deep neural networks, J. Comput. Phys. **399**, 108929 (2019).
[44] A. Rocchetto, E. Grant, S. Strelchuk, G. Carleo, and S. Severini, Learning hard quantum distributions with variational autoencoders, npj Quantum Inf. **4**, 1 (2018).
[45] M. Schmitt and M. Heyl, Quantum dynamics in transverse-field Ising models from classical networks, SciPost Phys. **4**, 013 (2018).
[46] R. Verdel, M. Schmitt, Y.-P. Huang, P. Karpov, and M. Heyl, Variational classical networks for dynamics in interacting quantum matter, Phys. Rev. B **103**, 165103 (2021).
[47] P. Karpov, R. Verdel, Y.-P. Huang, M. Schmitt, and M. Heyl, Disorder-Free Localization in an Interacting 2D Lattice Gauge Theory, Phys. Rev. Lett. **126**, 130401 (2021).
[48] T. Westerhout, N. Astrakhantsev, K. S. Tikhonov, M. I. Katsnelson, and, A. A. Bagrov, Generalization properties of neural network approximations to frustrated magnet ground states, Nat. Commun. **11**, 1593 (2020).
[49] P. Henelius and, A. W. Sandvik, Sign problem in Monte Carlo simulations of frustrated quantum spin systems, Phys. Rev. B **62**, 1102 (2000).
[50] D. Hangleiter, I. Roth, D. Nagaj, and J. Eisert, Easing the Monte Carlo sign problem, Sci. Adv. **6**, eabb8341 (2020).
[51] N. Hatano and M. Suzuki, Representation basis in quantum Monte Carlo calculations and the negative-sign problem, Phys. Lett. A **163**, 246 (1992).
[52] S. Dusuel, M. Kamfor, R. Orús, K. P. Schmidt, and J. Vidal, Robustness of a Perturbed Topological Phase, Phys. Rev. Lett. **106**, 107203 (2011).
[53] R. Kaubruegger, L. Pastori, and J. C. Budich, Chiral topological phases from artificial neural networks, Phys. Rev. B **97**, 195136 (2018).
[54] N. Astrakhantsev, T. Westerhout, A. Tiwari, K. Choo, A. Chen, M. H. Fischer, G. Carleo, and T. Neupert, Broken-Symmetry Ground States of the Heisenberg Model on the Pyrochlore Lattice, Phys. Rev. X **11**, 041021 (2021).
[55] A. Y. Kitaev, Fault-tolerant quantum computation by anyons, Ann. Phys. **303**, 2 (2003).
[56] D. Gottesman, Stabilizer codes and quantum error correction, Ph.D thesis, California Institute of Technology, 1997.
[57] D. A. Lidar and T. A. Brun, *Quantum Error Correction* (Cambridge University Press, Cambridge, UK, 2013).
[58] D. Gottesman, Theory of fault-tolerant quantum computation, Phys. Rev. A **57**, 127 (1998).
[59] C. K. Andersen, A. Remm, S. Lazar, S. Krinner, N. Lacroix, G. J. Norris, M. Gabureac, C. Eichler, and, A. Wallraff, Repeated quantum error detection in a surface code, Nat. Phys. **16**, 875 (2020).

[60] J. Vidal, R. Thomale, K. P. Schmidt, and S. Dusuel, Self-duality and bound states of the toric code model in a transverse field, Phys. Rev. B **80**, 081104(R) (2009).

[61] I. S. Tupitsyn, A. Kitaev, N. V. Prokof'ev, and P. C. E. Stamp, Topological multicritical point in the phase diagram of the toric code model and three-dimensional lattice gauge Higgs model, Phys. Rev. B **82**, 085114 (2010).

[62] F. Wu, Y. Deng, and N. Prokof'ev, Phase diagram of the toric code model in a parallel magnetic field, Phys. Rev. B **85**, 195104 (2012).

[63] J. Vidal, S. Dusuel, and K. P. Schmidt, Low-energy effective theory of the toric code model in a parallel magnetic field, Phys. Rev. B **79**, 033109 (2009).

[64] D.-L. Deng, X. Li, and S. D. Sarma, Machine learning topological states, Phys. Rev. B **96**, 195145 (2017).

[65] See Supplemental Material at http://link.aps.org/supplemental/10.1103/PhysRevResearch.4.L012010 for details on the cRBM architecture, topological phase transitions, the application to a frustrated system and the mapping to Tensor Network States.

[66] S. Sorella, M. Casula, and D. Rocca, Weak binding between two aromatic rings: Feeling the van der Waals attraction by quantum Monte Carlo methods, J. Chem. Phys. **127**, 014105 (2007).

[67] W. L. McMillan, Ground state of liquid He^4, Phys. Rev. **138**, A442 (1965).

[68] C.-Y. Park and M. J. Kastoryano, Geometry of learning neural quantum states, Phys. Rev. Research **2**, 023232 (2020).

[69] G. Carleo, K. Choo, D. Hofmann, J. E. T. Smith, T. Westerhout, F. Alet, E. J. Davis, S. Efthymiou, I. Glasser, S.-H. Lin *et al.*, Netket: A machine learning toolkit for many-body quantum systems, SoftwareX **10**, 100311 (2019).

[70] C. Castelnovo and C. Chamon, Quantum topological phase transition at the microscopic level, Phys. Rev. B **77**, 054433 (2008).

[71] P. Zanardi and N. Paunković, Ground state overlap and quantum phase transitions, Phys. Rev. E **74**, 031123 (2006).

[72] L. C. Venuti and P. Zanardi, Quantum Critical Scaling of the Geometric Tensors, Phys. Rev. Lett. **99**, 095701 (2007).

[73] A. Hamma, W. Zhang, S. Haas, and D. A. Lidar, Entanglement, fidelity, and topological entropy in a quantum phase transition to topological order, Phys. Rev. B **77**, 155111 (2008).

[74] A. Valenti, E. van Nieuwenburg, S. Huber, and E. Greplova, Hamiltonian learning for quantum error correction, Phys. Rev. Research **1**, 033092 (2019).

[75] M. B. Hastings, I. González, A. B. Kallin, and R. G. Melko, Measuring Renyi Entanglement Entropy in Quantum Monte Carlo Simulations, Phys. Rev. Lett. **104**, 157201 (2010).

[76] S. Sachdev, Quantum phase transitions, in *Handbook of Magnetism and Advanced Magnetic Materials* (Wiley, Hoboken, NJ, 2007).

[77] B. K. Chakrabarti, A. Dutta, and P. Sen, *Quantum Ising Phases and Transitions in Transverse Ising Models*, Lecture Notes in Physics Monographs Vol. 41 (Springer, Berlin, 2008).

[78] P. W. Leung and K. J. Runge, Spin-1/2 quantum antiferromagnets on the triangular lattice, Phys. Rev. B **47**, 5861 (1993).

[79] Y. Iqbal, W.-J. Hu, R. Thomale, D. Poilblanc, and F. Becca, Spin liquid nature in the Heisenberg J_1-J_2 triangular antiferromagnet, Phys. Rev. B **93**, 144411 (2016).

[80] L. Capriotti, A. E. Trumper, and S. Sorella, Long-Range Néel Order in the Triangular Heisenberg Model, Phys. Rev. Lett. **82**, 3899 (1999).

[81] S. Miyashita, A variational study of the ground state of frustrated quantum spin models, J. Phys. Soc. Jpn. **53**, 44 (1984).

[82] D. A. Huse and V. Elser, Simple Variational Wave Functions for Two-Dimensional Heisenberg Spin-1/2 Antiferromagnets, Phys. Rev. Lett. **60**, 2531 (1988).

[83] H. J. Schulz, T. A. L. Ziman, and D. Poilblanc, Magnetic order and disorder in the frustrated quantum Heisenberg antiferromagnet in two dimensions, J. Phys. I **6**, 675 (1996).

[84] F. Mezzacapo and J. I. Cirac, Ground-state properties of the spin-antiferromagnetic Heisenberg model on the triangular lattice: A variational study based on entangled-plaquette states, New J. Phys. **12**, 103039 (2010).

[85] Y. Huang and J. E. Moore, Neural Network Representation of Tensor Network and Chiral States, Phys. Rev. Lett. **127**, 170601 (2021).

[86] S. R. Clark, Unifying neural-network quantum states and correlator product states via tensor networks, J. Phys. A: Math. Theor. **51**, 135301 (2018).

[87] A. Valenti, E. Greplova, N. H. Lindner, and S. D. Huber, cRBM, https://github.com/cmt-qo/cm-cRBM, 2021.